Hindawi
Advances in Civil Engineering
Volume 2019, Article ID 6017146, 15 pages
https://doi.org/10.1155/2019/6017146

Research Article

A Heuristic Approach to Identify the Steel Grid Direction of R/C Slabs Using the Yield-Line Method for Analysis

Luigi Fenu,[1] Valeria Colasanti,[1] Eleonora Congiu,[1] Gian Felice Giaccu,[2] Francesco Trentadue,[3] and Bruno Briseghella[4]

[1]*Department of Civil and Environmental Engineering, and Architecture, University of Cagliari, Cagliari 09124, Italy*
[2]*Department of Architecture, Design and Urban Planning, University of Sassari, Alghero 07041, Italy*
[3]*Department of Civil Engineering and Architectural Science (DICAR), Technical University of Bari, Via Edoardo Orabona, 4, 70126 Bari, Italy*
[4]*College of Civil Engineering, Fuzhou University, No. 2 Xue Yuan Road, 350108 Fuzhou, Fujian Province, China*

Correspondence should be addressed to Bruno Briseghella; bruno@fzu.edu.cn

Received 26 April 2019; Revised 6 October 2019; Accepted 17 October 2019; Published 18 November 2019

Academic Editor: Hayri Baytan Ozmen

In the last few years, nonregular reinforced concrete (R/C) slabs have become more popular in buildings and bridges due to architectural or functional requirements. In these cases, an optimum design method to obtain the ultimate load capacity and the minimum reinforcement amount should be used. For simple R/C slabs, the yield-line method is extensively used in engineering practice. In addition to strength, the "true" failure mechanism is also obtained by identifying the parameters that define it and minimizing the collapse load. Unfortunately, when the mechanism is too complicated to be described or defined by several parameters (e.g., in slabs with complicated geometry), the method becomes more difficult because the system of nonlinear equations becomes harder to solve through traditional methods. In this case, an efficient and robust algorithm becomes necessary. In this paper, a structural analysis of R/C slabs is performed by using the yield-line method in association with a zero-th order optimization algorithm (the sequential simplex method) to avoid calculating gradients as well as any derivatives. The constraints that often limit these parameters are taken into account through the exterior penalty function method, leading to a successful solution of the problem. Considering that the direction of each yield-line is sought by minimizing the ultimate load and finding the parameters defining the collapse mechanism, another parameter concerned with the direction of an orthotropic reinforcement grid is introduced. In this way, the number of unknown parameters increases, but aside from obtaining the ultimate load and the parameters defining the collapse mechanism, the solution also finds both best and worst reinforcement orientations.

1. Introduction

Reinforced concrete (R/C) slabs with complex geometry are becoming a characteristic feature of many modern buildings and bridges. The yield-line method is often used in the design of R/C slabs at their ultimate load carrying capacity. Its reliability has been proven by many experimental tests conducted so far and by its widespread use [1–7]. Its main advantage is that it uses realistic collapse mechanism models and allows easy calculation in many simple applications. In these cases, after determining the typology of the collapse mechanism, meaning the number and form of the slab regions defined by the yield lines at ultimate, the virtual-work method is generally adopted to find the actual position of the yield lines and to calculate the ultimate load.

Unfortunately, when using the main mode of the virtual-work method, if the collapse mechanism is more complicated (for instance, when symmetry does not simplify the problem) and/or the number of parameters defining the collapse mechanism is high, complex nonlinear equations need to be solved to minimize the collapse load. Therefore, to use the yield-line method when a complex system of nonlinear equations is faced, efficient and robust zero-th order algorithms are required.

Zero-th order algorithms are particularly robust because they only use function values with no derivatives during the minimization process. Haftka and Gürdal [8] and Vanderplaats [9] described some applications of zero-th order methods in structural engineering. In the examples proposed in this study, the sequential simplex method was used. It is a zero-th order method originally defined by Spendley et al. [10] and improved by Nelder and Mead [11]. An application of the sequential simplex method to the optimum design of R/C structures by using the stringer-and-panel method was proposed by Biondini et al. [12], who applied it to an R/C supported beam. The use of the sequential simplex method for minimizing the ultimate load q_u is extensively described in [8].

In nonregular R/C slabs, it is necessary to identify the best reinforcement direction to minimize the used amount. In these cases, it can be useful to use the concept of structural optimization. It is well known that structural optimization is an important tool, both for sizing structure members and for helping the designer find the most suitable structural form [13–28]. Today, structural optimization is common in mechanical and aeronautical engineering, and in recent years it has been progressively adopted for structural-engineering applications, such as sizing building and bridge members [29–36], detailing reinforced concrete structures [37–45], shaping bridges [46–50], domes [51–54], and other three-dimensional structures [55].

Regarding concrete slabs, Kabir et al. [56] conducted an experimental and numerical study to investigate the effect of different directions of the reinforcement arrangements on the ultimate behaviour of skew slabs. Anderheggen [57] proposed a design approach for the reinforcement of concrete slabs and walls based on finite elements, plasticity theory, and linear programming. Lourenço and Figueras [58, 59] formulated a computational code based on equilibrium equations and an iterative procedure to design the reinforcement of plates and shells. Lourenço [60] referred to the three-layer sandwich model in Eurocode 2 to design plate and shell reinforcement with a linear analysis by finite elements [61, 62]. Mancini [63] and Bertagnoli et al. [64] studied the skew reinforcement design of two-dimensional elements in reinforced concrete by outlining two design problems to be resolved (choice of reinforcement direction and evaluation of reinforcement ratio for the chosen directions) and by using genetic algorithms for this purpose. Bertagnoli et al. [65, 66] also extended this optimum design approach based on genetic algorithms to concrete shells.

In this paper, a heuristic design approach using the yield-line method for analysis has been defined to identify the optimum reinforcement direction.

In Section 2, the considered parameters (i.e., slab boundaries, rotation axes of the slab regions delimited by the yield lines, and the degree of indetermination in assessing some of the rotation axes) for finding the collapse mechanism in the yield analysis are defined. The values of these parameters are obtained using a zero-th order optimization algorithm, which allows for finding the minimum of the ultimate load q_u without calculating its gradient. In so doing, a calculation that is not numerically robust can be avoided because the gradient calculation requires division by very small numbers close to zero. In Section 3, the method proposed to optimize the orientation of the reinforcement steel grid is introduced. A parameter describing its direction is defined, and the new objective function (i.e., the ultimate load) is minimized depending on this additional parameter, as well as on the parameters defining the yield line positions, the pattern of the yield lines, and the direction of the steel grid that further weaken the slab, which are also obtained. The stronger reinforcement is then superimposed in this direction, thus finding the best direction of the steel grid that better reinforces the slab and minimizes the ultimate load for the given optimum direction of the reinforcement grid. The method's efficacy is been demonstrated in a case study, performing a parametric optimization design of the slab reinforcement according to the grid orientation. Finally, conclusions are drawn.

2. R/C Slab Analysis through the Yield-Line Method Using an Optimization Algorithm

R/C slab analysis can be performed using the yield-line method if, on increasing the loads, the ductility is sufficiently high to allow the slab to become a mechanism at ultimate when the yield lines have already been completely developed. For R/C slabs currently used in civil engineering, a complete development of the yield lines can be attained when the reinforcement geometric ratio is less than approximately 1%; that is, at ultimate, the lever arm over the effective depth ratio is close to 0.9 [2]. Moreover, when using the yield-line analysis, a yield criterion for the reinforcement is needed: Johansen's criterion is herein assumed [67].

Consider an R/C slab with two orthogonal reinforcements, whose bars are spaced Δ in both directions and whose cross-sectional areas and effective depths are A_{s_x}, A_{s_y} and d_x, d_y, respectively. Say f_{yd} is the design yield strength of the reinforcement steel. The plastic moment in the two directions (the principal with stronger reinforcement, cross-sectional area A_{s_x}, effective depth d_x, and orthogonal one) can then be defined as

$$m_p = 0.9\left(\frac{A_{s_x}}{\Delta}\right) f_{yd} d_x,$$
$$\mu m_p = 0.9\left(\frac{A_{s_y}}{\Delta}\right) f_{yd} d_y, \tag{1}$$

with $\mu = A_{s_y} d_y / (A_{s_x} d_x)$.

For the virtual-work method, the external and internal work must be equal, namely,

$$L_{Est} = L_{Int}. \tag{2}$$

This equation relates the plastic moment of the stronger reinforcement and that in the orthogonal direction to the ultimate load q_u and the n parameters φ_i defining the collapse mechanism, that is, $m_p = f(\varphi_i, q_u)$ or, in a dual way, $q_u = g(\varphi_i, m_p)$, $i = 1, \ldots, n$.

Therefore, the problem is to find the n parameters φ_i that minimize q_u, that is, to solve the system:

$$\frac{\partial q_u}{\partial \varphi_i} = 0, \quad i = 1, \ldots, n. \tag{3}$$

System (3) can easily be solved through currently used methods (i.e., the substitution method), but only for simple cases, especially if simplified by symmetry, because q_u is a nonlinear function of φ_i, and system (3) is nonlinear as well. This system can instead become more complicated to be solved when the number n of parameters φ_i, and therefore the number of equations is increased. When the parameters are few but the objective function becomes more complex, as in the problem that will be investigated in the following section, the varying direction of the reinforcement grid makes system (3) more complicated to solve.

When applying the yield-line method with the virtual works to an R/C slab, the effective collapse mechanism is identified by defining some parameters φ_i, $i = 1, \ldots, n$, which depend on the collapse mechanism. The number n of parameters φ_i defining the collapse mechanism, and therefore, the pattern of the yield lines delimiting the slab regions, is determined by the slab boundaries, the rotation axes of the slab regions, as well as by the degree of indetermination in assessing some of the rotation axes.

Therefore, having assigned the arrangement of the reinforcement grid (for example, according to two orthogonal directions), and after solving system (3), the exact values of φ_i are found (and therefore the exact geometry of the mechanism), together with the actual value of the plastic moment m_p or, dually, of the ultimate load q_u.

Although the kinematic method provides an "upper bound" solution, its error is usually not very large, and its use is therefore allowed by many codes (i.e., Eurocode 2 [68]; ACI Code, see ACI Commentary 8.2.1 [69]).

2.1. Application of the Yield-Line Method Using an Unconstrained Optimization Algorithm. Consider, for instance, the trapezoidal R/C slab of Figure 1 with three supported edges, a free one, and a uniformly distributed load q.

This is a simple example of a nonsymmetrical concrete slab in which it is intuitive to conclude that the best direction of the reinforcement grid is not the one shown in Figure 1; although in practice, an engineering designer would likely place the grid with this orientation, that is, with the stronger reinforcement parallel to the free edge (Figure 1).

Therefore, it is assumed that an orthotropic grid of reinforcement bars (spaced Δ in both directions and with given reinforcement ratio μ) is placed along two orthogonal directions x and y. In this case, if the free edge and the other parallel sides are sufficiently long to not make the yield lines meet, the collapse mechanism is defined by determining the angles φ_1 and φ_2 formed between the direction orthogonal to the free edge and the two yield lines that define the three regions of the slab since there is no degree of indetermination in identifying their rotational axes.

Aside from the reinforcement grid, Figure 1 also shows the rotation axes of the three slab regions defined by the yield lines and the related rotation vectors ϑ_1, ϑ_2, and ϑ_3. The distance of the centroid of each slab region from its rotation axis is

$$d_{G1} = \frac{\Delta_1}{3}\sin\alpha,$$

$$d_{G2} = \frac{\Delta_2}{3}, \tag{4}$$

$$d_{G3} = \frac{B}{3}\,\frac{(3A/B) - 2(\tan\varphi_1 + \tan\varphi_2)}{(2A/B) - (\tan\varphi_1 + \tan\varphi_2)},$$

with $\Delta_1 = B(\cot\alpha + \tan\varphi_1)$ and $\Delta_2 = B\tan\varphi_2$.

Therefore, for each i-th slab region, say $S_{(i)}$, $\delta_{(i)}$, and $L_{\mathrm{Est}(i)} = (1/2)qS_{(i)}\delta_{(i)}$ denote the area, the centroid shift, and the work done by the external load q, respectively. For a unit shift of the free edge of the slab central region (Figure 2), when adding up the three external works in each slab region, the total external work is

$$L_{\mathrm{Est}} = \frac{1}{6}qB^2\left[3\frac{A}{B} - (\tan\varphi_1 + \cot\alpha + \tan\varphi_2)\right]. \tag{5}$$

The modules of the rotation vectors are

$$\vartheta_1 = \frac{1}{\Delta_1\sin\alpha},$$

$$\vartheta_2 = \frac{1}{\Delta_2}, \tag{6}$$

$$\vartheta_3 = \frac{1}{B},$$

and therefore, the internal work of the plastic moments m_p and μm_p in each slab region are, respectively,

$$\begin{aligned} L_{\mathrm{Int}(1)} &= m_p l_1\cos\varphi_1\cdot\vartheta_1 + \mu m_p l_1\sin\varphi_1\cdot\vartheta_1,\\ L_{\mathrm{Int}(2)} &= m_p l_2\cos\varphi_2\cdot\vartheta_2 + \mu m_p l_2\sin\varphi_2\cdot\vartheta_2,\\ L_{\mathrm{Int}(3)} &= m_p[l_1\cos\varphi_1 + l_2\cos\varphi_2]\cdot\vartheta_3\\ &\quad + \mu m_p[l_1\sin\varphi_1 + l_2\sin\varphi_2]\cdot\vartheta_3, \end{aligned} \tag{7}$$

where $l_1 = B/\cos\varphi_1$ and $l_2 = B/\cos\varphi_2$ are the lengths of the yield lines.

On summing these three contributions after calculating the scalar products, the total internal work is

$$L_{\mathrm{Int}} = m_p\left[\frac{B}{\Delta_1} + \frac{1}{\tan\varphi_2}\right] + \mu m_p\left[\tan\varphi_1\left(\frac{B\cot\alpha}{\Delta_1} - 1\right) - \tan\varphi_2\right]. \tag{8}$$

Therefore, the internal energy is dissipated in the slab to form the mechanism results, which are proportional to the plastic moment. Setting the total external work (5) equal to the total internal work (8) and extracting q_u, the objective function $q_u = q_u(\varphi_1, \varphi_2, m_p)$ is obtained, that is,

$$q_u = 6\frac{m_p}{B^2}\,\frac{B\tan\varphi_2 + \Delta_1 - \mu[\tan\varphi_1\tan\varphi_2(B\cot\alpha - \Delta_1) - \Delta_1\tan\varphi_2^2]}{\Delta_1\tan\varphi_2[3(A/B) - (\tan\varphi_1 + \tan\varphi_2) - \cot\alpha]}, \tag{9}$$

subject to the following constraints: $-(90^\circ - \alpha^\circ) \le \varphi_1 \le 90^\circ$, $0 \le \varphi_2 \le 90^\circ$, and $\Delta_1 + \Delta_2 \le A + B\cot\alpha$.

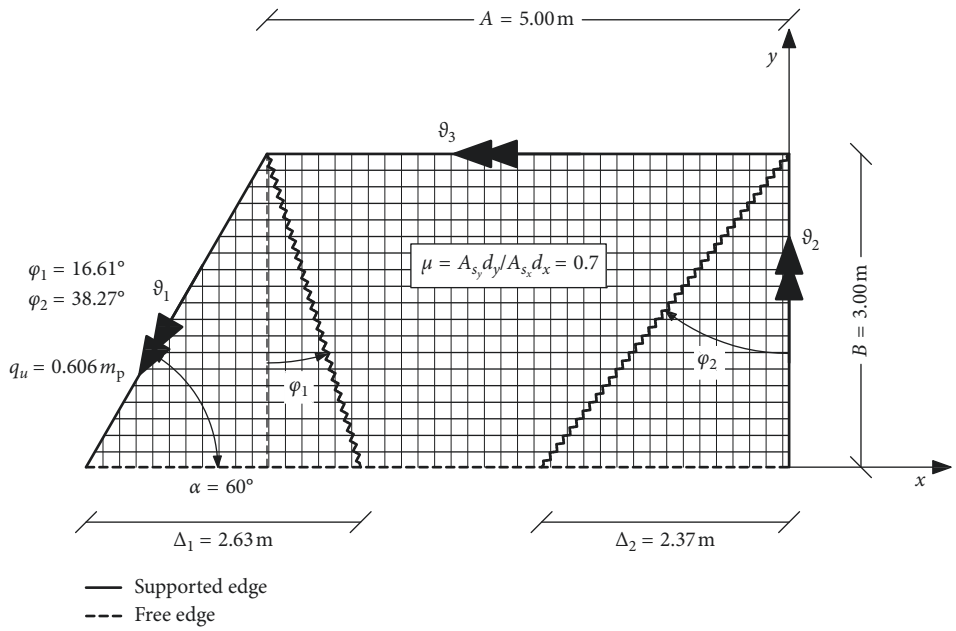

Figure 1: Trapezoidal R/C slab reinforced by a grid of steel bars with stronger reinforcement parallel to the free edge.

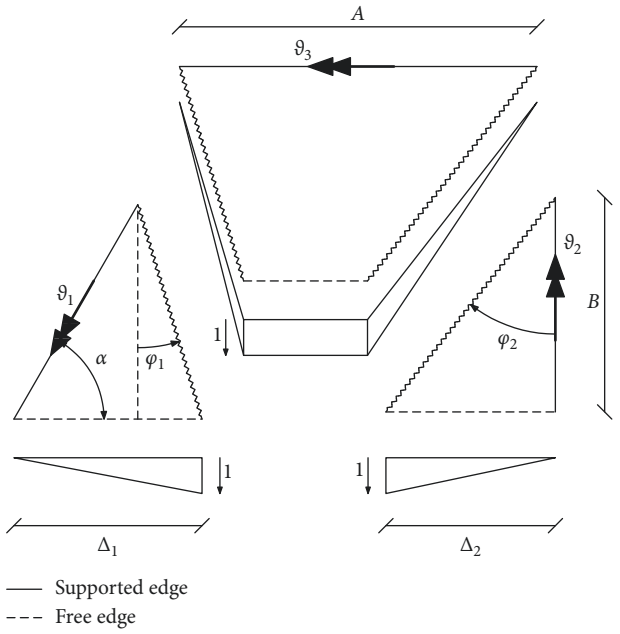

Figure 2: Virtual displacements of the slab regions.

It can be noted that while in this problem there are only two parameters, the nonlinear system (3) obtained through deriving equation (9) with respect to φ_1 and φ_2 is however not easy to solve. Therefore, traditional methods (such as the substitution method) cannot be adopted for this problem, and the use of an evolutionary optimization algorithm becomes usually necessary.

2.1.1. The Use of Zero-th Order Algorithms to Minimise the Objective Function: The Case of the Sequential Simplex Method. In this research, different evolutionary algorithms with zero-th order, such as genetic and particle swarm algorithms, as well as the sequential simplex method, have been considered. In solving the nonlinear system (3), different zero-th order algorithms have been compared, obtaining, as expected, very similar results. As a matter of fact, this holistic approach to optimizing the reinforcing grid inclination is only based on the physical laws governing the failure of concrete plates. Of course, different algorithms have different efficiencies and levels of robustness in solving system (3) but without affecting this holistic optimization method.

The sequential simplex method was originally proposed by Bhatt et al. [4] and improved by Ramsay and Johnson [5]. It is less robust than the genetic and particle swarm algorithms, but it is more efficient because, even if the gradient is not calculated (it is a zero-th order algorithm), the steepness of the objective function is considered.

In the analysed problem, the higher levels of robustness of the genetic and particle swarm algorithms were not quite as important due to the quick convergence, while the higher efficiency of the sequential simplex method was useful for saving computation time. The flowchart in Figure 3 shows how the sequential simplex method solves system (3) to minimize q_u.

The method starts by defining in the n-dimensional space O, $\varphi_1, \ldots, \varphi_n$ a simplex with $n+1$ vertices $\mathbf{x}_0$, $\mathbf{x}_1, \ldots, \mathbf{x}_n$, each of them defined by a vector $\mathbf{x}_i$ with n coordinates; the solution consists in finding the coordinate vector $\boldsymbol{\varphi} = [\varphi_1, \varphi_2, \ldots, \varphi_n]^T$ minimizing the function q_u and therefore maximizing the function m_p.

Consider $q_u = q_u(\varphi_i)$ in the n-dimensional space O, $\varphi_1, \ldots, \varphi_n$. In this space, a simplex is an $(n+1)$-faced polyhedral figure with $n+1$ vertices $0, 1, \ldots, n$. For example, in the three-dimensional space O, φ_1, φ_2, and φ_3, it is a tetrahedron with $3+1$ vertices and $3+1$ sides. If all the vertices have the same distance, we have a regular simplex.

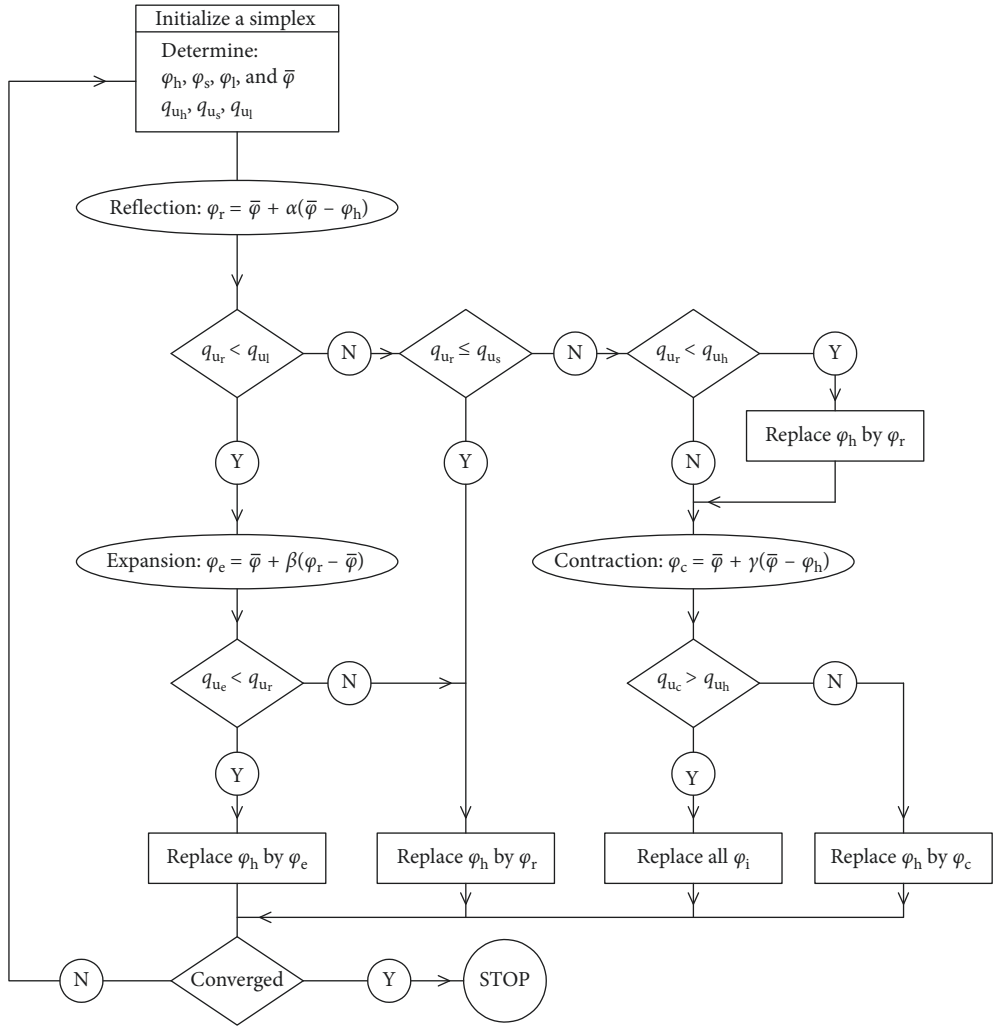

Figure 3: Flowchart of the sequential simplex method.

This means that in the two-dimensional space, the simplex is a triangle, and a regular simplex is an equilateral triangle. If $q_u = q_u(\varphi_i)$ is defined in the $O, \varphi_1, \ldots, \varphi_n$ space, $i = 1, \ldots, n$, then it has a real value in each simplex vertex $\mathbf{x}_0, \mathbf{x}_1, \ldots, \mathbf{x}_n$. Hence, if we find a simplex with a very small distance between these vertices, the smaller the better; the $n + 1$ values of q_u in the n vertices are very similar. This means that, if we implement an algorithm which finds these values very close to the minimum of the function q_u, then the minimum of q_u is considered as achieved, depending on the required precision, that is, on the maximum vertex distance which must be lower than a given small value.

Consider, for instance, the contour-plotted function in the O, φ_1, and φ_2 space of Figure 4, where the two simplices a and b are also defined. The simplex b is smaller than the simplex a, and the values of the function in each vertex of the simplex b are closer to the minimum than those of the simplex a. Starting from a simplex like the simplex a, the sequential simplex method searches for another simplex like the simplex b, where the function values (e.g., the values of function q_u) calculated at the simplex vertices are closer to the minimum than those of the vertices of the simplex a. Therefore, the smaller the simplex and the closer to the minimum function values at its vertices, the better is the approximation of the minimum function value.

Therefore, it must be implemented an algorithm that starting from an assigned simplex like a finds an enough small simplex like b whose vertex coordinates are sufficiently close to those that make q_u minimum. After the initial simplex has been defined, we evaluate q_u at each vertex finding two vertices $\mathbf{x}_l$ and $\mathbf{x}_h$ where q_u has the lowest and highest values (respectively, q_{u_l} and q_{u_h}), as well as a third vertex $\mathbf{x}_s$ where q_u has the second highest value q_{u_s}. Therefore, the algorithm will find the minimum of q_u discarding the vertex $\mathbf{x}_h$ where q_u is higher and replacing it with one point where it is lower. By doing so, a new simplex is defined whose new vertex $\mathbf{x}_h$ is also ready to be discarded when the function q_u takes on, in the subsequent simplex, a q_{u_h} value lower than in the simplex of the previous step. The operations that search for a new vertex for the new simplex are named reflection, contraction, and expansion. Discarded $\mathbf{x}_h$, reflection needs to find the centroid $\bar{\mathbf{x}}$ of the remaining vertices and to look for the new vertex $\mathbf{x}_r$ in the line joining $\mathbf{x}_h$ to $\bar{\mathbf{x}}$, namely, $\mathbf{x}_r = \bar{\mathbf{x}} + \alpha(\bar{\mathbf{x}} - \mathbf{x}_h)$, where α is usually

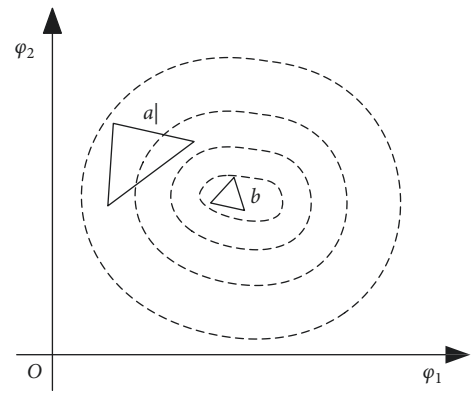

Figure 4: Contour-plotted function with the simplex a and the simplex b in a two-dimensional space.

assumed to be 1. Then, calculation of $q_{u_r} = q_u(\mathbf{x}_r)$ is needed. If $q_{u_l} < q_{u_r} \leq q_{u_h}$, this is good and $\mathbf{x}_r$ replaces $\mathbf{x}_h$. If $q_{u_r} < q_{u_l}$, this is better and we can try to further decrease q_u in a point $\mathbf{x}_e$ taken in the same direction by expansion, namely, $\mathbf{x}_e = \overline{\mathbf{x}} + \beta(\mathbf{x}_h - \overline{\mathbf{x}})$, where β is usually assumed to be 2. Now, if $q_{u_s} < q_{u_r}$, the expansion has attained its purpose and $\mathbf{x}_e$ replaces $\mathbf{x}_h$; otherwise, $\mathbf{x}_r$ will replace $\mathbf{x}_h$.

Finally, if $q_{u_s} < q_{u_r} < q_{u_h}$, after replacing $\mathbf{x}_h$ by $\mathbf{x}_r$, we make contraction finding $\mathbf{x}_c = \overline{\mathbf{x}} + \gamma(\mathbf{x}_h - \overline{\mathbf{x}})$, with $0 < \gamma < 1$ and usually chosen to be 1/2; otherwise $(q_{u_r} \geq q_{u_h})$, we make contraction with no replacement. After contraction, if $q_{u_e} > q_{u_h}$, the algorithm must be restarted after replacing all the vertices by a new set of points $\mathbf{x}_l = \mathbf{x}_i + (1/2)(\mathbf{x}_l - \mathbf{x}_i)$, $i = 0, 1, \ldots, n$; otherwise, we simply replace $\mathbf{x}_h$ by $\mathbf{x}_c$. After this whole process, we have defined a new simplex. In this way, at each step, the algorithm searches for a new simplex until the distance between the vertices is so small and q_{u_h} so close to q_{u_l} that convergence is reached when

$$\left(\frac{1}{1+n}\sum_{i=0}^{n}\left[q_{u_i} - q_u(\overline{\mathbf{x}})\right]^2\right)^{1/2} < \varepsilon, \tag{10}$$

the lower ε, the better.

By then considering the example of Figure 1, having defined the geometry of the trapezoidal R/C slab through assigning $A = 5.00$ m, $B = 3.00$ m, and $\alpha = 60^\circ$ and having assumed $\mu = 0.7$ for the ratio between weaker and stronger steel reinforcement and by using the optimization algorithm (i.e., the sequential simplex method), solving the system (3), one obtains $\varphi_1 = 16.61^\circ$ and $\varphi_2 = 38.27^\circ$ with $\Delta_1 = 2.63$ m and $\Delta_2 = 2.37$ m, and $q_u = 0.606\, m_p$. The total internal energy L_{Int} per unit m_p dissipated in the slab to form the mechanism is 3.033. The plot of the unconstrained objective function (9) for $A = 5.00$ m, $B = 3.00$ m, $\alpha = 60^\circ$, and $\mu = 0.7$ is shown in Figure 5.

2.2. Application of the Yield-Line Method Using a Constrained Optimization Algorithm. When evaluating q_u, the variable φ_i, $i = 1, \ldots, n$, may have to be constrained. In fact, to respect the assigned mechanism, some φ_i could be defined only in a specific interval and/or an expression containing some variables could be limited.

In general, the function q_u can be subject to both unequal constraints $s_j(\boldsymbol{\varphi}) \leq 0$, $j = 1, \ldots, m$ and equal constraints $h_k(\boldsymbol{\varphi}) = 0$, $k = 1, \ldots, l$. These constraints can be taken into account through a penalty function $P(\boldsymbol{\varphi})$. Some constrained structural engineering problems solved by using penalty function methods are shown by Cetin et al. [20].

Using virtual works in the yield-line method, the exterior penalty function method can be incorporated in the sequential simplex method. To this aim, a penalty function $P(\boldsymbol{\varphi})$ is added to the function $q_u(\boldsymbol{\varphi})$, thus obtaining the new function

$$\Phi\left(\boldsymbol{\varphi}, r_p\right) = q_u(\boldsymbol{\varphi}) + r_p P(\boldsymbol{\varphi}), \tag{11}$$

where $\Phi(\boldsymbol{\varphi}, r_p)$ is named the pseudo-objective function and r_p is a scalar multiplier much higher than 1 (namely, in this kind of problems, chosen to be between 100 and 1000), while the m unequal constraints $s_j(\boldsymbol{\varphi}) \leq 0$ and the l equal constraints $h_k(\boldsymbol{\varphi}) = 0$ are taken into account through the exterior penalty function $P(\boldsymbol{\varphi})$:

$$P(\boldsymbol{\varphi}) = \sum_{j=1}^{m}\left[max\left[0,\, s_j(\boldsymbol{\varphi})\right]\right]^2 + \sum_{k=1}^{l}\left[h_k(\boldsymbol{\varphi})\right]^2. \tag{12}$$

If the constraints are not violated at any point near the minimum, the penalty function $P(\boldsymbol{\varphi})$ is not active, its value is zero, and $\Phi(\boldsymbol{\varphi}, r_p) = q_u(\boldsymbol{\varphi})$. This is the case of unconstrained problems, where, depending on the mechanism typology, q_u reaches its minimum without being constrained.

On the contrary, if $\Phi(\boldsymbol{\varphi}, r_p)$ is constrained when reaching the minimum, the penalty function $P(\boldsymbol{\varphi})$ becomes active. This means that at the points where the constraints are violated, q_u cannot reach its unconstrained minimum because the related mechanism is not possible and the problem is not defined (i.e., the mechanism of Figure 6(b)). In this case, the penalty function $P(\boldsymbol{\varphi})$ assumes a positive real value when violating the relative constraint, thus making $\Phi(\boldsymbol{\varphi}, r_p)$ increase greatly, also depending on the chosen value of r_p.

Actually, by assigning different dimensions to the slab of Figure 1, q_u do not always reach its unconstrained minimum with the previously assigned mechanism. Therefore, in this case, the constraints to the objective function q_u become active.

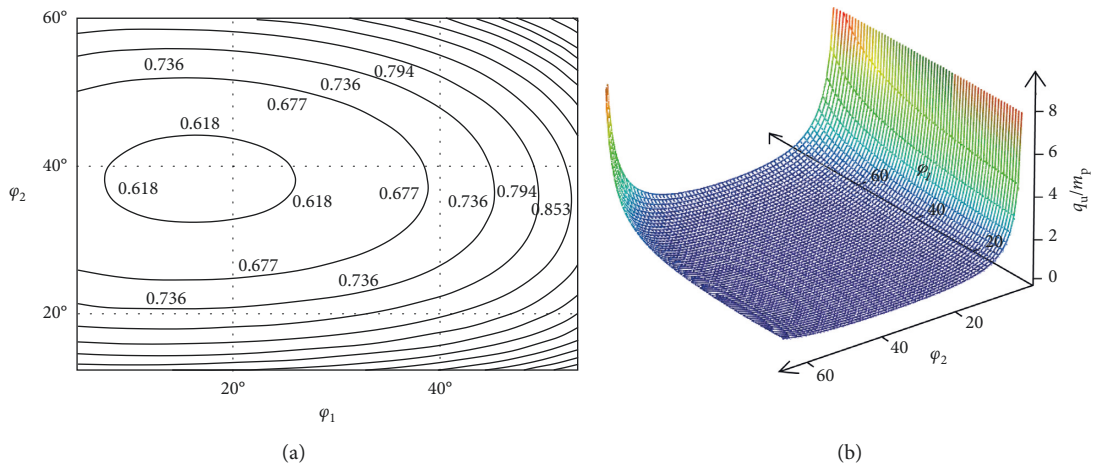

FIGURE 5: Contour plot (a) and 3D diagram (b) of the objective function q_u calculated for the slab of Figure 1.

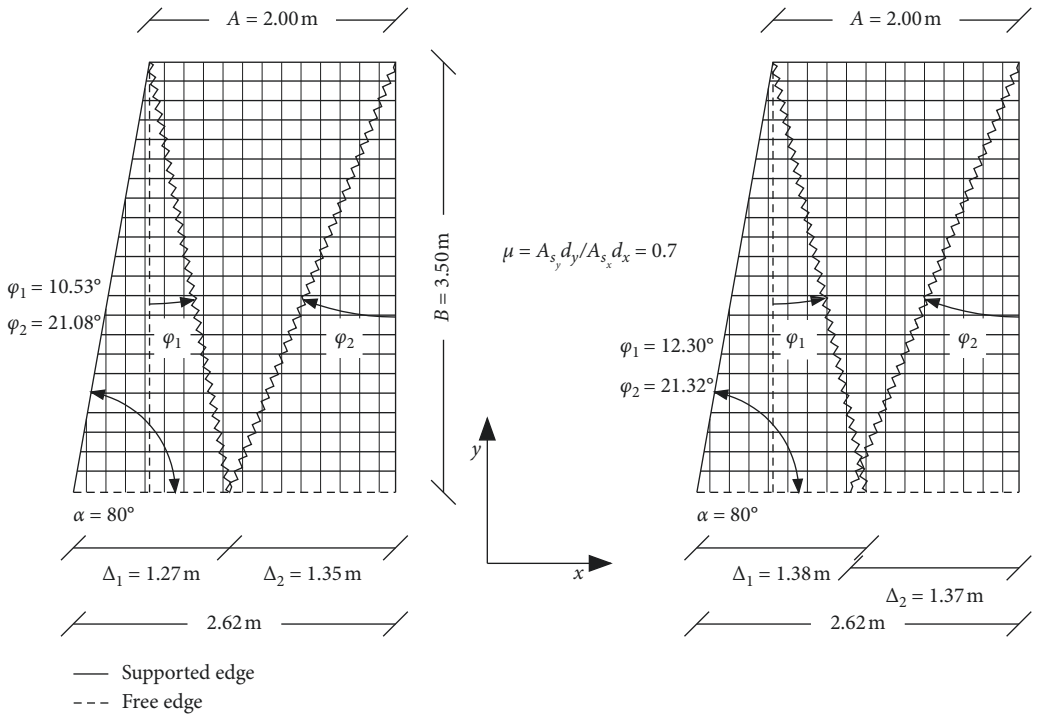

FIGURE 6: Effect of the penalty function coupled to the sequential simplex method when using the yield-line method for analysis of a trapezoidal R/C slab. (a) Constrained solution. The pseudo-objective function value is $\Phi(\varphi_1 = 10.53°; \varphi_2 = 21.08°) = 0.347$ with $P(x) = 0$. (b) Unconstrained solution kinematically inadmissible. The pseudo-objective function value after incrementing the parameter values of one degree $\Rightarrow P(\boldsymbol{\varphi}) \neq 0$ and $\Phi(\varphi_1 = 11.53°; \varphi_2 = 22.08°; r_p = 100) = 2.037$.

For instance, this occurs for a trapezoidal R/C slab, similar to the previous one with $\mu = 0.7$, but with $A = 2.00\,m$, $B = 3.50\,m$, and $\alpha = 80°$ (Figure 6). In this case, using the sequential simplex method coupled with the exterior penalty function method, one obtains $q_u = 2.170\,m_p$ with $\varphi_1 = 10.53°$, $\varphi_2 = 21.08°$ and with $\Delta_1 = 1.27\,m$, $\Delta_2 = 1.35\,m$. The length of the free edge $A + B\cot\alpha = 2.62\,m$ is equal to the sum $\Delta_1 + \Delta_2$. In other words, a constrained minimum is reached with $\Phi = 0.347$ for a unitary value of m_p and $P(\varphi_i) = 0$ (Figure 6(a)). This means that the penalty function has automatically discarded solutions with $\Delta_1 + \Delta_2 > A + B\cot\alpha$. In fact, disregarding the constraints, that is without coupling any penalty function to the objective function, the unconstrained minimum would have been reached with $\varphi_1 = 12.30°$, $\varphi_2 = 21.32°$, $\Delta_1 = 1.38\,m$, $\Delta_2 = 1.37\,m$, and $\Delta_1 + \Delta_2 = 2.75\,m$. However, this is impossible because the constraint $\Delta_1 + \Delta_2 \leq A + B\cot\alpha$ would have been violated and another slab region, kinematically inadmissible, would have been generated (Figure 6(b)). By instead increasing the parameter values $\varphi_1 = 10.53°$ and $\varphi_2 = 21.08°$ obtained in the constrained solution (i.e., by adding one degree to each parameter), that is, setting $\varphi_1 = 11.53°$

and $\varphi_2 = 22.08^\circ$, the violation of the constraint makes $P(\varphi_i) \neq 0$, thus greatly increasing the pseudo-objective function $\Phi(\varphi_i, r_p)$. For instance, for $r_p = 100$, one obtains $\Phi(\varphi_1 = 11.53^\circ, \varphi_2 = 22.08^\circ, r_p = 100) = 2.037$, which is almost six times the value $\Phi = 0.347$ obtained in the minimum, meaning that the solution found is actually a constrained solution.

Therefore, having assigned the mechanism, if q_u reaches its unconstrained minimum and, on slightly increasing the parameters, we still have $P(\boldsymbol{\varphi}) = 0$ and $\Phi(\boldsymbol{\varphi}, r_p) = q_u(\boldsymbol{\varphi})$; then, the collapse mechanism does not need to be constrained, and no penalty function would be necessary. Otherwise, when q_u reaches a constrained minimum, a slight increase of the parameters leads to $P(\boldsymbol{\varphi}) \neq 0$. In this case, the penalty function becomes active, thus highly increasing $\Phi(\boldsymbol{\varphi}, r_p)$. This means that, in general, the collapse mechanism must be constrained in order to find the actual solution.

It must be noted that, for the given mechanism with one inner trapezoidal slab region and two lateral triangular ones, the constrained minimum of Figure 6(a) led to three triangular slab regions where the inner trapezoidal region diverged into a triangular one. This constrained minimum was reached after having seen that lower values of φ_1 and φ_2 led to higher values of the objective function q_u.

Nevertheless, does q_u attain the constrained minimum for this diverged mechanism with three triangular slab regions? No, it cannot, because this would be true for the given mechanism, but the kinematic analysis shows that the slab also admits another failure mechanism with an inner triangular slab region and two lateral trapezoidal ones having a side in common intersecting the free side of the slab (Figure 7). For kinematic reasons, this side in common must lie on a straight line passing on the point where the rotation axes of the two trapezoidal slab regions meet each other. This means that in this mechanism, the two yield lines defining the triangular region are always constrained to meet each other along the straight line passing through two points: the first one where these two yield lines meet and the second one where the lines overlapping the rotation axes of the two trapezoidal slab regions meet each other (Figure 7).

The kinematically admissible mechanisms of this problem are hence two, a first one with the inner trapezoidal region and two lateral triangular regions (i.e., in Figure 1) and a second one with the inner triangular region and two lateral trapezoidal regions (Figure 7). Therefore, the minimum of q_u must be searched for both mechanisms by varying φ_1 and φ_2 without violating the constraints. For both mechanisms, the optimization algorithm will search for the minimum of q_u for $\varphi_1 > 0$ and $\varphi_2 > 0$ until, in both cases, the mechanism diverges forming three triangular slab regions.

Similarly to the first mechanism and following the same procedure, when considering the second mechanism illustrated in Figure 7, the total internal work is to be obtained by adding the internal works calculated for each of the three slab regions. For this aim, the direction of their rotation vectors ϑ_i, $i = 1, \ldots, 3$, and their plastic moments m_{p_i} and μm_{p_i} are to be evaluated, as well as the magnitude of the rotation vectors ϑ_i.

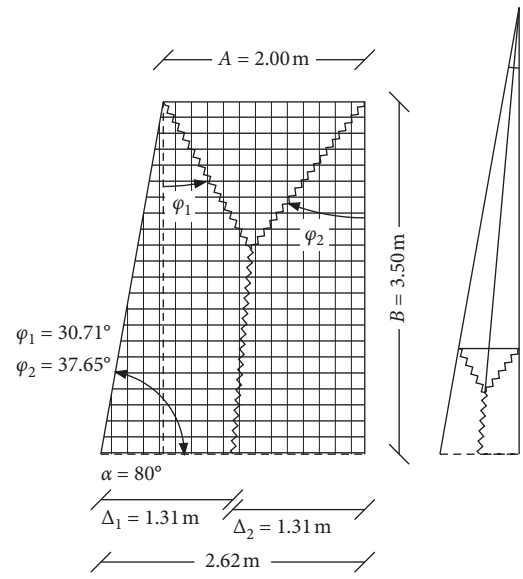

Figure 7: Failure mechanism with an inner triangular slab region and two lateral trapezoidal ones having a side in common intersecting the free side.

After identifying the centroid of each slab region, the three related external works are evaluated and added to each other to obtain the total external work. By then adding the total internal work to the total external work, the objective function $q_u(\varphi_1, \varphi_2)$ is explicited and minimized through using the sequential simplex method.

The results show that for the slab dimensions in Figures 3 and 7, the minimum q_u is obtained for $\varphi_1 = 30.71^\circ$ and $\varphi_2 = 37.65^\circ$ with $\Delta_1 = \Delta_2 = 1.31$ m. This yield-line pattern occurs for $q_u = 1.891\, m_p$. This ultimate load is thus lower than $2.17\, m_p$, previously obtained from the other mechanism at its boundary for which also its inner trapezoidal slab region becomes triangular. This means that this first mechanism cannot occur for $q_u/m_p = 2.17$ because for $q_u/m_p = 1.891$, the slab would have already failed with the second mechanism shown in Figure 7.

3. Choice of the Best Reinforcement Direction

Since the yield-line method locates the narrow bands in the slab where plastic deformations are concentrated, and the yield lines are therefore spontaneously selected by the mechanism as "weakness" lines in the slab at yield, this method can be suitably extended to determine the most unfavourable reinforcement arrangement, that is, the "weakest" slab reinforcement arrangement at yield with the lowest ultimate load q_u.

A heuristic optimization method for determining the best direction of the reinforcement grid is hence proposed. The grid orientation is indicated through a further parameter whose most unfavourable value is, in general, unknown. Since the mechanism is identified through n unknown parameters φ_i, $i = 1, \ldots, n$, this further unknown parameter φ_{n+1} increases the number of unknowns by 1. Therefore, $n + 1$ equations are needed to identify the values of all the $n + 1$ unknown parameters.

Therefore, through a heuristic point of view, once the parameter φ_{n+1} is known, the stronger reinforcement A_{s_x} should replace the weaker reinforcement A_{s_y} and vice versa, thus giving the best orientation to the reinforcement grid. The simple example described in the following section illustrates the application of this heuristic optimization method.

3.1. An Example of the Application of the Proposed Heuristic Optimization Method for Identifying the Best Grid Orientation by Using the Yield-Line Method for Analysis. Consider another simple example of a slab similar to the previous one in Figure 1, only differing from it by the orientation of the reinforcement grid that, in general, can be at an angle to the free edge, identified by an additional parameter φ_3. Therefore, φ_3 is also the slope to the direction orthogonal to the free edge of the weaker reinforcement with area A_{s_y} and direction y (Figure 8).

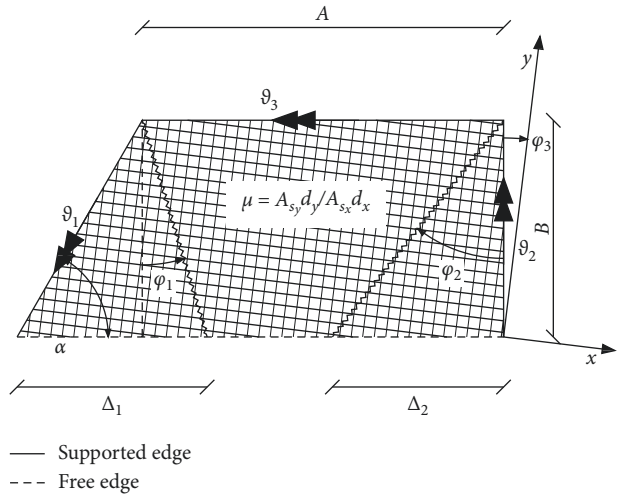

Figure 8: Trapezoidal R/C slab with reinforcement grid at an angle to the free edge. The angle between direction y of the weaker reinforcement and the direction at a right angle to the free edge is φ_3, assumed as an additional parameter in the optimization algorithm.

Figure 9 shows the three slab regions of the slab of Figure 8 separately, their respective rotation axes with the related rotation vectors ϑ_1, ϑ_2, and ϑ_3, as well as the plastic moments m_p and μm_p along the yield lines. The distance of the centroid of each slab region from its rotation axis, the modulus of the rotation vectors, and therefore the total external work is also, of course, the same as that of the slab in Figure 1 with the given reinforcement direction. For each of the three slab regions in Figure 9, the internal works of the plastic moments m_p and μm_p are

$$\begin{aligned} L_{\mathrm{Int}(1)} &= m_p l_1 \cos(\varphi_1 + \varphi_3) \cdot \vartheta_1 + \mu m_p l_1 \sin(\varphi_1 + \varphi_3) \cdot \vartheta_1, \\ L_{\mathrm{Int}(2)} &= m_p l_2 \cos(\varphi_2 - \varphi_3) \cdot \vartheta_2 + \mu m_p l_2 \sin(\varphi_2 - \varphi_3) \cdot \vartheta_2, \\ L_{\mathrm{Int}(3)} &= m_p [l_1 \cos(\varphi_1 + \varphi_3) + l_2 \cos(\varphi_2 - \varphi_3)] \cdot \vartheta_3 \\ &\quad + \mu m_p [l_1 \sin(\varphi_1 + \varphi_3) + l_2 \sin(\varphi_2 - \varphi_3)] \cdot \vartheta_3. \end{aligned} \tag{13}$$

On summing up these three contributions, the total internal work is

$$\begin{aligned} L_{\mathrm{Int}} &= m_p \left[\frac{\cos(\varphi_1 + \varphi_3)}{\cos\varphi_1} \left(\frac{\sin(\alpha + \varphi_3)}{\Delta_1 \sin\alpha} - \frac{\sin\varphi_3}{B} \right) + \frac{\cos(\varphi_2 - \varphi_3)}{\cos\varphi_2} \left(\frac{\cos\varphi_3}{\Delta_2} + \frac{\sin\varphi_3}{B} \right) \right] B \\ &\quad + \mu m_p \left[\frac{\sin(\varphi_1 + \varphi_3)}{\cos\varphi_1} \left(\frac{\cos\varphi_3}{B} - \frac{\cos(\alpha + \varphi_3)}{\Delta_1 \sin\alpha} \right) + \frac{\sin(\varphi_2 - \varphi_3)}{\cos\varphi_2} \left(\frac{\cos\varphi_3}{B} - \frac{\sin\varphi_3}{\Delta_2} \right) \right] B. \end{aligned} \tag{14}$$

By setting up the total external work equal to the total internal work and extracting q_u, the objective function $q_u = q_u(\varphi_1, \varphi_2, \varphi_3, m_p)$, subject to the three constraints $-(90^\circ - \alpha^\circ) \le \varphi_1$, $0 \le \varphi_2$, and $\Delta_1 + \Delta_2 \le A + B\cot\alpha$, is obtained.

Minimizing q_u, one obtains $\varphi_1 = 9.67^\circ$, $\varphi_2 = 33.18^\circ$, and $\varphi_3 = 107.69^\circ$ with $\Delta_1 = 2.24$ m, $\Delta_2 = 1.96$ m, and $q_u = 0.486\, m_p$. The total internal energy L_{Int} per unit m_p is 2.625 (Figure 10).

This means that the mechanism has spontaneously selected the slab's "weakness" lines (yield lines), thus identifying their positions through the angles φ_1 and φ_2, as well as the position of the weaker reinforcement A_{s_y}. Therefore, supposing an absurd scenario where someone wants to weaken the slab, the weaker reinforcement should be placed at an angle $\varphi_3 = 107.69^\circ$ to the direction orthogonal to the free edge (Figure 10).

Once the reinforcement grid orientation that would weaken the slab is identified, if one instead wants to better reinforce the slab, the stronger reinforcement A_{s_x} must be positioned in place of the weaker (that is, at an angle of 107.69° in the direction at a right angle to the free edge), thus positioning the weaker reinforcement A_{s_y} with an inclination $\varphi_3 = 17.69^\circ$, that is, shifted 90° from the y direction

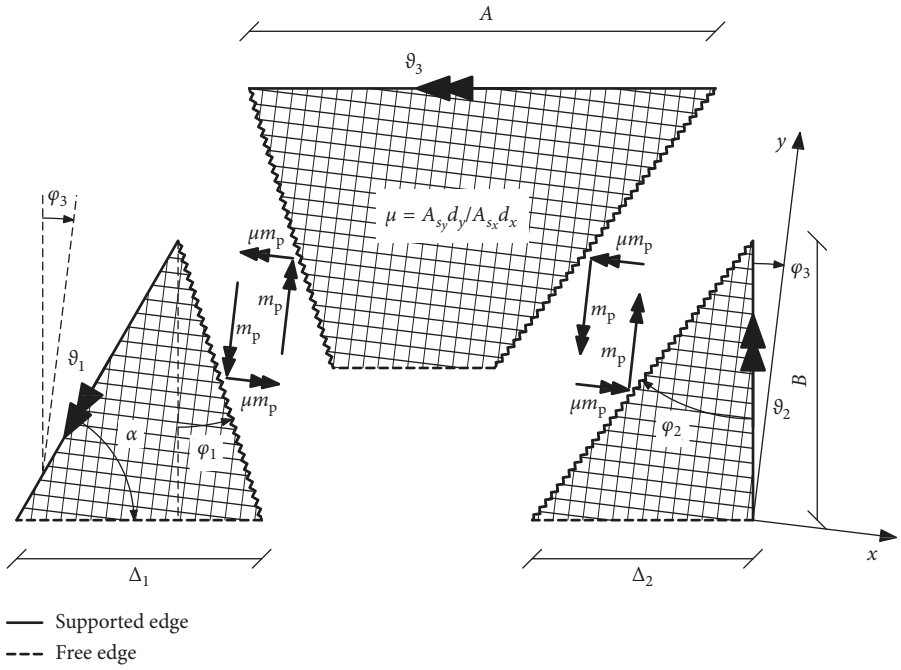

Figure 9: Slab regions with the reinforcement at an angle to the free edge.

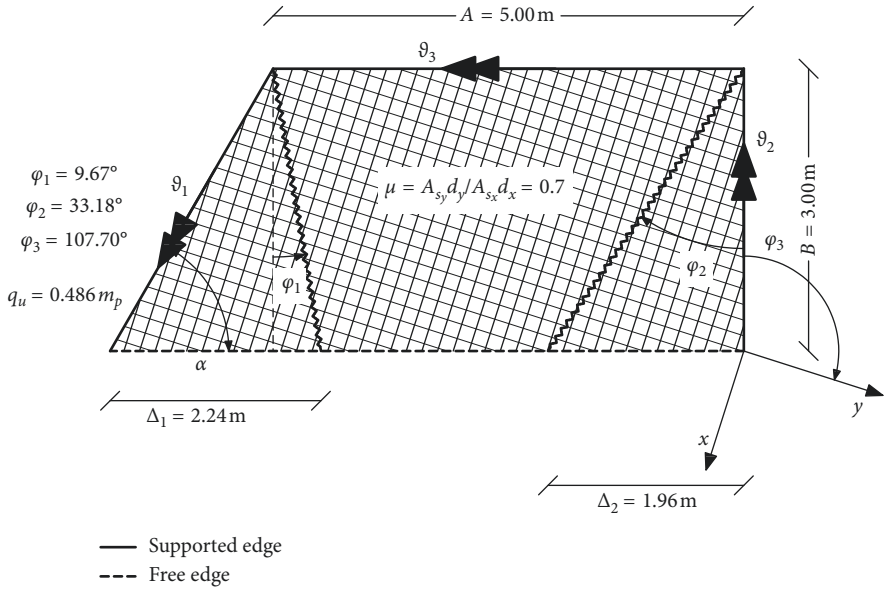

Figure 10: Most unfavourable reinforcement arrangement.

($\varphi_3 = 107.69°$), previously obtained through the sequential simplex method.

In other words, contrary to what is required by the algorithm in order to weaken the slab, to better reinforce the slab, the reinforcement A_{s_x} must be positioned in place of A_{s_y}, that is, with an inclination of 17.69° to the free edge and the slab side orthogonal to the free edge (see Figure 11). The ultimate load related to this best reinforcement arrangement is then obtained by minimizing the objective function $q_u = q_u(\varphi_1, \varphi_2, \varphi_3 = 17.69°, m_p)$ by using the optimization algorithm but with only the two variables, φ_2 for a given φ_3. It is thus found that $\varphi_1 = 17.39°$ and $\varphi_2 = 37.44°$ (with $\Delta_1 = 2.67$ m, $\Delta_2 = 2.30$ m), when $q_u = 0.620\,m_p$. The ratio L_{Int} over m_p becomes 3.112.

This simple example demonstrates that, as expected, the best reinforcement arrangement has the stronger reinforcement A_{s_x}, not parallel to the free edge but at an angle of 17.69°.

The main aim of the simple example herein illustrated is to better explain the proposed heuristic optimization method. It is worth highlighting that when the algorithm is used with three parameters, it searches for the minimum of

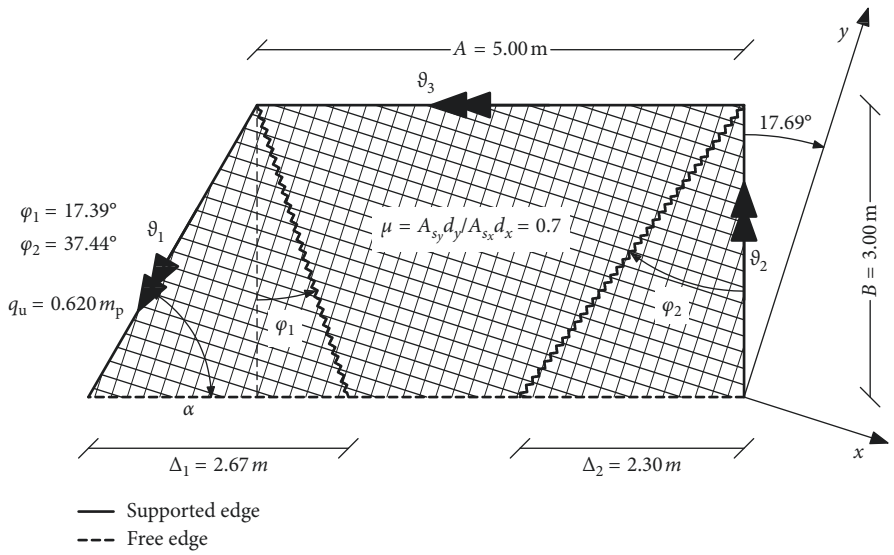

Figure 11: Most favourable reinforcement arrangement.

q_u, while also choosing the most unfavourable orientation φ_3 of the reinforcement grid. Conversely, when two parameters are used, the algorithm searches for the minimum of q_u for a given grid orientation, that is, for a given value of φ_3. By then allowing φ_3 to vary in the interval [0°, 180°] or symmetrically in the interval [0°, −180°] (the two variation intervals refer to the same grid orientations, see Figure 12), a parametric design of the orientation of the reinforcement grid can be performed. In so doing, after evaluating the ultimate load for any given value of φ_3 (that is, the ratio q_u/m_p as a function of φ_3), the optimum grid orientation can be determined. The results of the parametric design are shown in Figure 12. As previously obtained through the proposed optimization method, the minimum of q_u/m_p actually occurs for $\varphi_3 = 107.69°$ and, symmetrically, for $\varphi_3 = -71.31°$, i.e., for the same grid orientation. Conversely, the maximum of q_u/m_p is obtained for φ_3 shifted by 90°, that is, for $\varphi_3 = 17.69°$, meaning that the parametric optimization confirms the results obtained through the proposed heuristic optimization method.

The other grid orientations considered in Figure 12 lead to intermediate values of the ratio q_u/m_p, shown to vary sinusoidally with φ_3. The diagram shows that by taking a unit value of m_p, the maximum value of q_u is approximately 27.5% higher than the minimum. The reinforcement arrangement in Figure 1 with $\varphi_3 = 0$ and a stronger steel parallel to the free edge demonstrates a good efficiency, with q_u/m_p being only 2.5% lower than the maximum (Figure 12).

Finally, the cross-sectional area and the spacing of the grid reinforcement bars can be calculated. For this aim, let us assume a slab thickness at 14 cm (for instance, $d_x = 10$ cm and a cover of 4 cm). The design value of the steel yield strength can be assumed to be $f_{yd} = 391$ MPa that can be referred to as $f_{yk} = 450$ MPa, B450 for Eurocode 2. The design factored load $q_{ud} = 12.35\ \text{kN/m}^2$ is also assumed.

Considering the optimum direction of the steel grid ($\varphi_3 = 17.69°$), the required cross-sectional area per unit length of the stronger reinforcement is determined to be

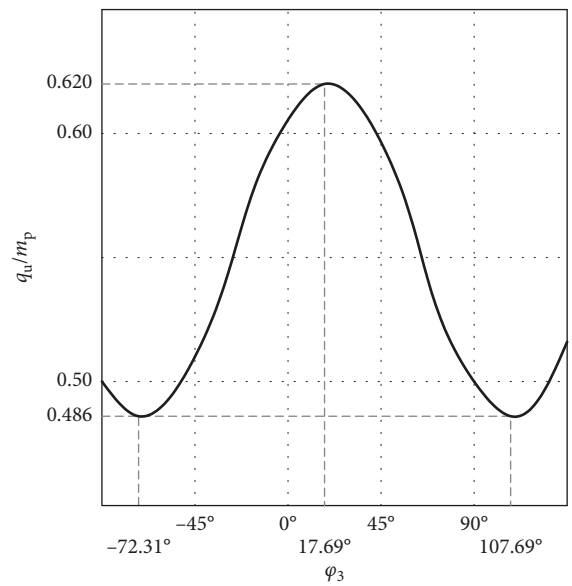

Figure 12: Variation of the q_u/m_p ratio as a function of φ_3.

$A_{s_x\text{req}} = q_{ud}/(0.620 \cdot f_{yd} \cdot 0.9 \cdot d_x) = 5.66\ \text{cm}^2/\text{m}$ so that an actual stronger reinforcement $A_{s_x} = \phi 12/20$ cm can be provided. By instead considering the reinforcement grid in Figure 1 ($\varphi_3 = 0°$), a reinforcement $A_{s_x\text{req}} = 5.85\ \text{cm}^2/\text{m}$ parallel to the free edge is required so that the bar spacing must be reduced to 19 cm for the same bar diameter $\phi 12$. Therefore, having assumed a reinforcement ratio $\mu = 0.7$, since the ratio between the cross-sectional area of bars $\phi 12$ and bars $\phi 10$ is 0.695 (that is, almost 0.7), the provided weaker reinforcement A_{s_y} is then $\phi 10/20$ cm and $\phi 10/19$ cm for $\varphi_3 = 17.69°$ and $\varphi_3 = 0°$, respectively. As expected, by comparing the steel weights of these two reinforcement arrangements, the weight of the optimum one is approximately 2.5% lower than that of the other, as it happens for the ratio q_u/m_p.

The same goal is achieved for the trapezoidal slab of Figure 7 with variable orientation of the reinforcement grid failing by the second mechanism considered in the previous section. Of course, the rotation axes position and direction are not affected by the variable orientation of the reinforcement grid. Moreover, for any φ_3 including the grid orientation considered in the slab of Figure 7, the magnitude of the rotation vectors ϑ_1, ϑ_2, and ϑ_3 does not vary by varying φ_1 and φ_2. The directions of the plastic moments m_{p_i} and μm_{p_i} are instead affected by the variation of the grid orientation. After evaluating the external and the internal works, following the procedure of the previous example of this section, the objective function $q_u = q_u(\varphi_1, \varphi_2, \varphi_3, m_p)$ is obtained. It is subject to the constraints $-(90^\circ - \alpha^\circ) \le \varphi_1$, $0 \le \varphi_2$, and $\Delta_1 + \Delta_2 \le A + B\cot\alpha$. For the dimensions of the slab of Figure 7, by minimizing q_u, one obtains that the grid orientation more weakening the slab is $\varphi_3 = 95.30^\circ$, meaning that the weaker reinforcement A_{s_y}, initially parallel to the y-axis, rotates of an angle $\varphi_3 = 95.30$ in the clockwise direction to weaken the slab as much as possible. The stronger reinforcement A_{s_x} is then positioned in place of the weaker A_{s_y}, that is, at an angle of 5.30° in the clockwise direction with respect to the x-axis (Figure 13). The inclination to the y-axis of the weaker reinforcement A_{s_y} is thus 5.30°, that is, shifted 90° from the direction previously obtained through minimizing the function $q_u = q_u(\varphi_1, \varphi_2, \varphi_3, m_p)$. For given $\varphi_3 = 5.30^\circ$, the ultimate load q_u related to this best grid orientation is then obtained by minimizing the objective function $q_u = q_u(\varphi_1, \varphi_2, \varphi_3 = 5.30^\circ, m_p)$ with only the two variables φ_1 and φ_2 for given $\varphi_3 = 5.30^\circ$. One obtains $q_u = 1.906\, m_p$ with the yield-line pattern identified by $\varphi_1 = 30.56^\circ$, $\varphi_2 = 37.06^\circ$ (with $\Delta_1 = 1.30$ m, $\Delta_2 = 1.32$ m). It can be noted that, as expected, in this case, the ratio of the ultimate load $q_u = 1.906 m_p$ of the slab with optimum grid orientation $\varphi_3 = 5.30^\circ$ over the ultimate load $q_u = 1.891\, m_p$ of the slab with $\varphi_3 = 0^\circ$ is 0.99, that is, higher than in the previous case of the slab of Figure 1. Of course, this ratio tends to 1 for α tending to 90°, that is, when the trapezoidal slab tends to become a rectangular slab.

Regarding the saving of construction materials, the results obtained in the example (approximately 2-3%) are related to the analysed geometry and are comparable to other studies, for example, by Mancini [63] and by Bertagnoli et al. [66]. In large structures, even a small improvement could yield a significant saving of construction materials. A greater material saving from 5 to 10% can be obtained for different geometries, especially in complex buildings that are becoming quite frequent in contemporary architecture. This was confirmed by the research performed by Kabir et al. [56], whose work both numerically and experimentally investigated the effect of varying the direction of the reinforcements of skew slabs. They found that the best reinforcement orientation can improve the ultimate load up to 10%, thus leading to a proportional increase of the plastic moment, which means for a given ultimate load, there is an equivalent saving of the reinforcement cross-sectional area and steel weight.

The structural design of contemporary architecture will likely require procedures for designing the reinforcement of concrete slabs with complex geometry, with an increasing amount of concrete slabs needing not only optimization of the reinforcement direction and of steel weight but also optimization of the production method, as in innovative tailor-made concrete structures [70] with all slabs having different reinforcement arrangements.

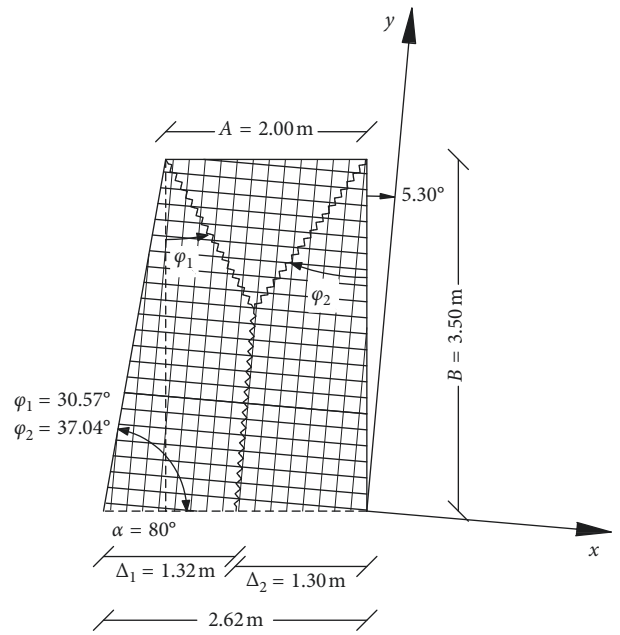

Figure 13: Optimum grid orientation for the slab of Figure 7.

4. Conclusions

The use of the virtual-work method within the yield-line approach is generally advantageous because while providing an "upper bound" solution, it is usually sufficiently precise. In addition to the ultimate load, it also provides the exact collapse mechanism of the slab. Unfortunately, even when there is not a prohibitive number of unknown parameters defining the collapse mechanism, the nonlinear equation system defining the problem is difficult to solve through traditional methods.

Therefore, a robust and efficient algorithm is needed. These difficulties have been avoided by using the sequential simplex method, a zero-th order algorithm that is proven not only to be robust but also very efficient. Since this algorithm is efficient and robust and is slightly influenced by the increase in the number of parameters defining the collapse mechanism, in this paper, the yield-line method was extended by adding a further parameter defining the direction of the reinforcement grid. In fact, since the yield lines are narrow bands in the slab where plastic deformations are concentrated and whose actual position minimizes the ultimate load with respect to any other possible position, when the ultimate load is minimized as a function of both the position of the yield lines and the orientation of the reinforcement grid, this additional parameter identifies the most unfavourable orientation of the reinforcement grid

corresponding to the minimum of the ultimate load. This means that the yield-line method can identify not only the orientation of the yield lines that minimize the ultimate load (that, therefore, further "weakens" the slab) but also the orientation of the reinforcement grid that, by contributing to minimizing the ultimate load, must be the most unfavourable among all the possible grid orientations, thus "weakening" the slab as much as possible.

In so doing, it was possible to heuristically optimize the grid's orientation through positioning the stronger reinforcement in place of the weaker one by rotating the reinforcement grid by 90°. Therefore, the optimization algorithm (i.e., any optimization algorithm as the sequential simplex method used in this study) searches for the worst reinforcement grid orientation (the one for which the ultimate load is minimum), while the heuristic optimization method herein proposed finds the best grid orientation, which is the one for which the ultimate load is at a maximum.

The method has shown to be effective at optimizing the reinforcement direction in R/C slabs, as confirmed by the subsequently performed parametric design. In fact, for any possible orientation of the reinforcement grid, the yield-line method was used for the analysis of the R/C slab by assigning the grid orientation at each time. The results confirm those obtained through the heuristic optimization method herein proposed. Since at each stage and for each grid orientation, this parametric optimization procedure is performed using the yield-line method for analysis in its currently used application without any additional parameters accounting for the reinforcement direction; the results of the parametric optimization reliably confirm those of the heuristic optimization procedure.

Data Availability

The data used to support the findings of this study are included within the article.

Conflicts of Interest

The authors declare that they have no conflicts of interest.

Acknowledgments

This research was supported by the National Natural Science Foundation of China (grant no. 51778148), by the Recruitment Program of Global Experts Foundation (grant no. TM2012-27), and by the FIR fund 2016-17 of the University of Cagliari. The authors would like to acknowledge the Sustainable and Innovative Bridge Engineering Research Center (SIBERC) of the College of Civil Engineering, Fuzhou University (Fuzhou, China) and the Department of Civil Engineering, Environmental Engineering, and Architecture of the University of Cagliari (Cagliari, Italy).

Supplementary Materials

Supplementary file shows the research highlights. (*Supplementary Materials*)

References

[1] C. Massonnet and M. A. Save, *Calcul Plastique des Constructions*, Center Belgian-Luxembourgeois d'Information de l'Acier, Brussels, Belgium, 1963.

[2] R. Favre, J. P. Jaccoud, M. Koprna, and A. Radojicic, *Dimensionnement des Structures en béton: Aptitude au Service et éléments de Structures*, Presses polytechniques et universitaires romandes, Lausanne (Suisse), Switzerland, 1990.

[3] R. Park, W. L. Gamble, and L. William, *Reinforced Concrete Slabs*, Wiley, New York, NY, USA, 2000.

[4] P. Bhatt, T. J. MacGinely, and B. S. Choo, *Reinforced Concrete Design to Eurocodes, Design Theory and Examples*, CRC Press Inc, Boca Raton, FL, USA, 2014.

[5] A. C. A. Ramsay and D. Johnson, "Analysis of practical slab configurations using automated yield-line analysis and geometric optimization of fracture patterns," *Engineering Structures*, vol. 20, no. 8, pp. 647–654, 1998.

[6] A. Ramsay, E. Maunder, and M. Gilbert, "Modern limit analysis tools for reinforced concrete slabs," *Structure Magazine*, vol. 9, pp. 31–33, 2015.

[7] M. Gilbert, L. He, C. C. Smith, and C. V. Le, "Automatic yield-line analysis of slabs using discontinuity layout optimization," *Proceedings of the Royal Society A: Mathematical, Physical and Engineering Sciences*, vol. 470, no. 2168, p. 20140071, 2014.

[8] R. T. Haftka and Z. Gürdal, "Elements of structural optimization," in *Solid Mechanics And Its Applications*, vol. 11Dordrecht, Netherlands, Kluwer Academic Publishers, 1993.

[9] G. N. Vanderplaats, *Numerical Optimization Techniques for Engineering Design : With Applications*, McGraw-Hill, New York, NY, USA, 1984.

[10] W. Spendley, G. R. Hext, and F. R. Himsworth, "Sequential application of simplex designs in optimisation and evolutionary operation," *Technometrics*, vol. 4, no. 4, pp. 441–461, 1962.

[11] J. A. Nelder and R. Mead, "A simplex method for function minimization," *The Computer Journal*, vol. 7, no. 4, pp. 308–313, 1965.

[12] F. Biondini, F. Bontempi, P. G. Malerba, and A. Simone, "Optimal reinforcement layout in concrete elements by using the stringer and panel method," in *Proceeding of the Fourth International Colloquium on Structural Morphology*, Delft, Netherlands, 2000.

[13] Y. S. Shin, R. T. Haftka, L. T. Watson, and R. H. Plaut, "Design of laminated plates for maximum buckling load," *Journal of Composite Materials*, vol. 23, no. 4, pp. 348–369, 1989.

[14] M. Kripka, G. F. Medeiros, and A. C. C. Lemonge, "Use of optimization for automatic grouping of beam cross-section dimensions in reinforced concrete building structures," *Engineering Structures*, vol. 99, pp. 311–318, 2015.

[15] N. D. Lagaros, M. Fragiadakis, M. Papadrakakis, and Y. Tsompanakis, "Structural optimization: a tool for evaluating seismic design procedures," *Engineering Structures*, vol. 28, no. 12, pp. 1623–1633, 2006.

[16] D. Lavorato, C. Nuti, S. Santini, B. Briseghella, and J. Xue, "A repair and retrofitting intervention to improve plastic dissipation and shear strength of Chinese rc bridges," *IABSE Symposium Report*, vol. 105, no. 9, pp. 1–6, 2015.

[17] L. Fenu, G. C. Marano, E. Congiu, and B. Briseghella, *Steel Truss-type Arches Optimization under Multi-Load Cases*, IABSE Congress, New York City, NY, USA, 2019.

[18] L. Fenu, G. C. Marano, E. Congiu, and B. Briseghella, "Optimum design of an arched truss under vertical and horizontal

multi-load cases," in *Joint Conference Form and Force, IASS 60th Anniversary Symposium (IASS Symposium 2019) 8th International Conference on Textile Composites and Inflatable Structures (Structural Membranes 2019)*, Barcelona, Spain, 2019.

[19] H. Cetin, E. Aydin, and B. Ozturk, "Optimal damper allocation in shear buildings with tuned mass dampers and viscous dampers," *International Journal of Earthquake and Impact Engineering*, vol. 2, no. 2, p. 89, 2017.

[20] H. Cetin, E. Aydin, and B. Ozturk, "Optimal design and distribution of viscous dampers for shear building structures under seismic excitations," *Frontiers in Built Environment*, vol. 5, pp. 1–13, 2019.

[21] S. Adriaenssens, P. Block, D. Veenendaal, and C. Williams, *Shell Structures for Architecture*, Taylor & Francis- Routledge, London, UK, 2014.

[22] M. P. Bendsoe, "Optimal shape design as a material distribution problem," *Structural Optimization*, vol. 1, no. 4, pp. 193–202, 1989.

[23] G. I. N. Rozvany, M. Zhou, and T. Birker, "Generalized shape optimization without homogenization," *Structural Optimization*, vol. 4, no. 3-4, pp. 250–252, 1992.

[24] D. Veenendaal and P. Block, "An overview and comparison of structural form finding methods for general networks," *International Journal of Solids and Structures*, vol. 49, no. 26, pp. 3741–3753, 2012.

[25] G. C. Marano, F. Trentadue, and F. Petrone, "Optimal arch shape solution under static vertical loads," *Acta Mechanica*, vol. 225, no. 3, pp. 679–686, 2014.

[26] L. Fenu, B. Bruno, and G. C. Marano, "Optimum shape and length of laterally loaded piles," *Structural Engineering and Mechanics*, vol. 68, pp. 121–130, 2018.

[27] C. Lan, B. Briseghella, L. Fenu, J. Xue, and T. Zordan, "The optimal shapes of piles in integral abutment bridges," *Journal of Traffic and Transportation Engineering (English Edition)*, vol. 4, no. 6, pp. 576–593, 2017.

[28] F. Trentadue, G. C. Marano, I. Vanzi, and B. Briseghella, "Optimal arches shape for single-point-supported deck bridges," *Acta Mechanica*, vol. 229, no. 5, pp. 2291–2297, 2018.

[29] L. L. Stromberg, A. Beghini, W. F. Baker, and G. H. Paulino, "Topology optimization for braced frames: combining continuum and beam/column elements," *Engineering Structures*, vol. 37, pp. 106–124, 2012.

[30] X. Huang and Y. M. Xie, "Topology optimization of nonlinear structures under displacement loading," *Engineering Structures*, vol. 30, no. 7, pp. 2057–2068, 2008.

[31] A. P. Thrall, S. Adriaenssens, I. Paya-Zaforteza, and T. P. Zoli, "Linkage-based movable bridges: design methodology and three novel forms," *Engineering Structures*, vol. 37, pp. 214–223, 2012.

[32] T. Zordan, E. Mazzarolo, B. Briseghella et al., "Optimization of calatrava bridge in Venice," in *Bridge Maintenance, Safety, Management and Life Extension*, pp. 1863–1869, CRC Press, Boca Raton, FL, USA, 2014.

[33] B. Briseghella, L. Fenu, C. Lan, E. Mazzarolo, and T. Zordan, "Application of topological optimization to bridge design," *Journal of Bridge Engineering*, vol. 18, no. 8, pp. 790–800, 2013.

[34] T. Zordan, B. Briseghella, and E. Mazzarolo, "Bridge structural optimization through step-by-step evolutionary process," *Structural Engineering International*, vol. 20, no. 1, pp. 72–78, 2010.

[35] Q. Q. Liang, Y. M. Xie, and G. P. Steven, "Optimal topology design of bracing systems for multistory steel frames," *Journal of Structural Engineering*, vol. 126, no. 7, pp. 823–829, 2000.

[36] G. K. Georgoussis, "Preliminary structural design of wall-frame systems for optimum torsional response," *International Journal of Concrete Structures and Materials*, vol. 11, no. 1, pp. 45–58, 2017.

[37] M. H. F. M. Barros, R. A. F. Martins, and A. F. M. Barros, "Cost optimization of singly and doubly reinforced concrete beams with EC2-2001," *Structural and Multidisciplinary Optimization*, vol. 30, no. 3, pp. 236–242, 2005.

[38] C. C. Ferreira, M. H. F. M. Barros, and A. F. M. Barros, "Optimal design of reinforced concrete T-sections in bending," *Engineering Structures*, vol. 25, no. 7, pp. 951–964, 2003.

[39] M. Di Prisco, M. Mauri, and M. Scola, "On the optimal design of precast structural elements: a proposal," *Studies and Research, Graduate School in Concrete Structures, Politecnico di Milano*, vol. 24, pp. 77–119, 2003.

[40] G. Quaranta, A. Fiore, and G. C. Marano, "Optimum design of prestressed concrete beams using constrained differential evolution algorithm," *Structural and Multidisciplinary Optimization*, vol. 49, no. 3, pp. 441–453, 2014.

[41] A. Scodeggio, G. Quaranta, G. C. Marano, G. Monti, and R. B. Fleischman, "Optimization of force-limiting seismic devices connecting structural subsystems," *Computers & Structures*, vol. 162, pp. 16–27, 2016.

[42] G. C. Marano, F. Trentadue, and R. Greco, "Optimum design criteria for elastic structures subject to random dynamic loads," *Engineering Optimization*, vol. 38, no. 7, pp. 853–871, 2006.

[43] G. C. Marano, F. Trentadue, and R. Greco, "Stochastic optimum design criterion of added viscous dampers for buildings seismic protection," *Structural Engineering and Mechanics*, vol. 25, no. 1, pp. 21–37, 2007.

[44] R. Greco, A. Lucchini, and G. C. Marano, "Robust design of tuned mass dampers installed on multi-degree-of-freedom structures subjected to seismic action," *Engineering Optimization*, vol. 47, no. 8, pp. 1009–1030, 2015.

[45] G. Quaranta, G. C. Marano, R. Greco, and G. Monti, "Parametric identification of seismic isolators using differential evolution and particle swarm optimization," *Applied Soft Computing*, vol. 22, pp. 458–464, 2014.

[46] B. Briseghella, L. Fenu, Y. Feng, E. Mazzarolo, and T. Zordan, "Topology optimization of bridges supported by a concrete shell," *Structural Engineering International*, vol. 23, no. 3, pp. 285–294, 2013.

[47] B. Briseghella, L. Fenu, Y. Feng, C. Lan, E. Mazzarolo, and T. Zordan, "Optimization indexes to identify the optimal design solution of shell-supported bridges," *Journal of Bridge Engineering*, vol. 21, no. 3, Article ID 04015067, 2016.

[48] L. Fenu, B. Briseghella, and T. Zordan, "Curved shell-supported footbridges," *IABSE Symposium Report*, vol. 105, no. 43, pp. 1–8, 2015.

[49] L. Fenu, E. Congiu, and B. Briseghella, "Curved deck arch bridges supported by an inclined arch," in *19th IABSE Congr.*, pp. 21–23, Stockholm, Sweden, 2016.

[50] L. Fenu, B. Briseghella, and E. Congiu, "Curved footbridges supported by a shell obtained as an envelope of thrust-lines," in *ARCH'16 - 6th Int. Conf. Arch Bridg.*, Wroclaw Univ. Technol., Wroclaw, Poland, 2016.

[51] P. Block, *Thrust Network Analysis : Exploring Three-Dimensional Equilibrium*, Massachusetts Institute of Technology, Cambridge, MA, USA, 2009.

[52] F. Marmo and L. Rosati, "Reformulation and extension of the thrust network analysis," *Computers & Structures*, vol. 182, pp. 104–118, 2017.

[53] B. Maurin and R. Motro, "Concrete shells form-finding with surface stress density method," *Journal of Structural Engineering*, vol. 130, no. 6, pp. 961–968, 2004.

[54] C. Chang and A. Chen, "The gradient projection method for structural topology optimization including density-dependent force," *Structural and Multidisciplinary Optimization*, vol. 50, no. 4, pp. 645–657, 2014.

[55] A. N. Christiansen, J. A. Bærentzen, M. Nobel-Jørgensen, N. Aage, and O. Sigmund, "Combined shape and topology optimization of 3D structures," *Computers & Graphics*, vol. 46, pp. 25–35, 2015.

[56] A. Kabir, SM. Nizamud-Doulah, and M. Kamruzzaman, "Effective reinforcement layout for skew slabs A. 27th Conf," in *Proceedings of the 27th Conference on Our World In Concrete & Structures*, Singapore, August 2002.

[57] E. Anderheggen, "Finite elements, plasticity theory and linear programming for dimensioning reinforced concrete slabs and walls," in *Trends in Structural Mechanics*, vol. 54, pp. 225–234, Springer, Dordrecht, Netherlands, 1997.

[58] P. B. Lourenço and J. A. Figueiras, "Automatic design of reinforcement in concrete plates and shells," *Engineering Computations*, vol. 10, no. 6, pp. 519–541, 1993.

[59] P. B. Lourenço and J. A. Figueiras, "Solution for the design of reinforced concrete plates and shells," *Journal of Structural Engineering*, vol. 121, no. 5, pp. 815–823, 1995.

[60] P. B. Lourenço, "Reinforcement design using linear analysis," in *Plates FEM Suprises Pitfalls*, J. Blaauwendraad, Ed., pp. 291–318, Springer Science+Business Media, Berlin, Germany, 2010.

[61] EN 1992-2 Eurocode 2, *Design of Concrete Structures—Part 2: Concrete Bridges—Design and Detailing Rules*, UNI—Ente Nazionale Italiano di Unificazione, Milan, Italy, 2005.

[62] International Federation for Structural Concrete (fib), *Practitioners' Guide to Finite Element Modelling of Reinforced Concrete Structures—State-Of-Art Report*, International Federation for Structural Concrete (fib), Lausanne, Switzerland, 2008.

[63] G. Mancini, "From modeling to design of concrete structures," in *Int. Symp. Innov. Sustain*, L. Zhitao, W. Zhishen, L. Aiqun et al., Eds., Struct. Civ. Eng., 2005.

[64] G. Bertagnoli, V. I. Carbone, L. Giordano, and G. Mancini, "Skew reinforcement design in reinforced concrete two dimensional elements," in *Proceedings of the Second International Specialty Conference on the Conceptual Approach to Structural Design*, pp. 283–290, Milan, Italy, 2003.

[65] G. Bertagnoli, L. Giordano, and S. Mancini, "Design and optimization of skew reinforcement in concrete shells," *Structural Concrete*, vol. 13, no. 4, pp. 248–258, 2012.

[66] G. Bertagnoli, L. Giordano, and S. Mancini, "A metaheuristic approach to skew reinforcement optimization in concrete shells under multiple loading conditions," *Structural Engineering International*, vol. 24, no. 2, pp. 201–210, 2014.

[67] K. W. Johansen, *Yield-Line Theory*, Cement and Concrete Association, London, UK, 1962.

[68] EN 1992-1-1 Eurocode 2, *Design of Concrete Structures—Part 1-1: General Rules and Rules for Buildings—5.6.2 Plastic Analysis for Beams, Frames and Slabs*, UNI—Ente Nazionale Italiano di Unificazione, Milan, Italy, 2005.

[69] ACI, Building Code Requirements for Reinforced Concrete (ACI 318-14)—Commentary on Building Code Requirements for Structural Concrete (ACI 318R-14), American Concrete Institute, Farmington Hills, MI, USA, 2011.

[70] D. Fall, K. Lundgren, R. Rempling, and K. Gylltoft, "Reinforcing tailor-made concrete structures: alternatives and challenges," *Engineering Structures*, vol. 44, pp. 372–378, 2012.